Increased Cortical Oxidative Metabolism Due to Sensory Stimulation: Implications for Functional Brain Imaging

Ivo Vanzetta and Amiram Grinvald

Modern functional brain mapping relies on interactions of neuronal electrical activity with the cortical microcirculation. The existence of a highly localized, stimulus-evoked initial deoxygenation has remained a controversy. Here, the activity-dependent oxygen tension changes in the microcirculation were measured directly, using oxygen-dependent phosphorescence quenching of an exogenous indicator. The first event after sensory stimulation was an increase in oxygen consumption, followed by an increase in blood flow. Because oxygen consumption and neuronal activity are colocalized but the delayed blood flow is not, functional magnetic resonance imaging focused on this initial phase will yield much higher spatial resolution, ultimately enabling the noninvasive visualization of fundamental processing modules in the human brain.

Understanding of human cognitive brain function has greatly improved with the emergence of noninvasive methodologies for high-resolution functional neuroimaging, such as positron emission tomography (PET) and functional magnetic resonance imaging (fMRI). These techniques have allowed the rapid identification of functionally distinct cortical areas (*1, 2*). Moreover, the study of the layout of individual cortical modules (*3*) within a given brain area and their geometrical relationships (*4*) has become feasible using the much higher spatial resolution of optical imaging based on intrinsic signals. These three methods monitor regional changes in cerebral blood flow and blood oxygenation level, relying on the coupling between local electrical activity and cerebral microcirculation (*2, 5, 6*).

Previous optical imaging experiments have argued that sensory-evoked electrical activity gives rise to a highly localized initial increase in oxygen consumption. This leads to an increase in the concentration of deoxyhemoglobin, followed by a deoxyhemoglobin decrease caused by a delayed blood flow increase, which is not well regulated at the level of cortical functional domains (*7*). This interpretation has been further supported by optical imaging spectroscopy (*8*). The initial increase in deoxyhemoglobin concentration, referred to as the initial dip, was recently confirmed by high-field fMRI measurements at 4 to 9.4 T (*9, 10*). However, the large majority of low-field BOLD (blood oxygenation level–dependent) fMRI measurements, as well as other methodologies, have not detected the initial dip (*11, 12*) or have found only a minimal increase in oxygen consumption (*6, 13*).

This apparent contradiction raises the question of what is actually being measured by the BOLD effect or by optical imaging spectroscopy. Mayhew and colleagues (*12*) have argued that a problem exists with the interpretation of previous imaging spectroscopy data (*8*), claiming that the linear model used was oversimplified and may have introduced large errors in the calculated deoxyhemoglobin time course. We share the opinion that the selected model, as well as assumptions about some of its parameters, are indeed critical (*14*). In addition, our imaging spectroscopy measurements had a time resolution of 500 ms, thus providing timing precision of ~1 s. This time resolution is not sufficient to monitor the sequence of very early changes in oxy- or deoxyhemoglobin concentration and blood volume (*8*) and their temporal relationship to blood flow changes (*7*). Therefore, to resolve this controversy, we decided to bypass imaging spectroscopy by measuring microvascular oxygen concentration changes directly, at a time resolution improved by a factor of 5.

To this end, we measured the phosphorescence decay of Oxyphor R2 [Pd-meso-tetra(4-carboxyphenyl) porphyrin dendrimer] in the cerebral microcirculation. Oxyphor R2 is an oxygen tension–sensitive phosphorescent probe that, once injected intravenously, associates with albumin and thus does not leak out of the microcirculation. This method, introduced by Wilson and colleagues (*15–17*), is based on the fact that phosphorescence can be quenched by molecular oxygen. Thus, phosphorescence lifetime can be used to directly measure rapid changes in the oxygen concentration in the probe's immediate environment.

To detect the oxygen concentration changes, we first injected anesthetized cats with the oxygen-sensitive phosphorescent probe intravenously at 30 mg/kg of body weight (*18*). The exposed cortex was implanted with a cranial window and illuminated by brief flashes at 10 Hz (width ~2 μs at half-height) using standard epi-illumination via the objective lens of the macroscope (*19*). The emitted phosphorescence was detected by a photomultiplier (Fig. 1A). The known drop in oxygen concentration during barbiturate anesthesia (*20*) causes a considerably longer lifetime (Fig. 1B). This result indicates that the measurement can be done in the living brain. Remarkably, the small changes in decay time in response to sensory stimulation were reliably detected as well (Fig. 1C). The emergent order in the set of decay curves, each obtained at a different time with respect to the visual stimulus, proves that changes in the phosphorescence decay times can clearly be detected in response to the sensory stimulation. The phosphorescence decay time becomes longer 1.4 s after stimulus onset (Fig. 1D), which suggests that after sensory activation of the cortex, there is a rapid decrease in the microvascular free oxygen concentration. Several alternative interpretations for the observed change in decay time, critically discussed in previous in vivo and in vitro applications of this technique (*16, 17*), have been ruled out here (*21*). Therefore, we conclude that the slower decay curve observed after 1.4 s was indeed due to the activity-induced decrease in the microvascular oxygen tension, resulting from an increased oxygen consumption.

To obtain the time course of relative changes in oxygen concentration, we used signal averaging and calculated the decay times for every flash (*22*). The results (Fig. 2A) show a biphasic curve: Immediately after the stimulus onset, the phosphorescence decay time becomes longer, and then it begins to decline and undershoots after ~2.5 s. As a control, we measured the changes in the phosphorescence decay time in the absence of a visual stimulus. The flat line thus obtained (Fig. 2A, thin line) underscores the reliability of these decay time measurements.

The kinetics of the oxygen concentration changes can be derived from these decay times using the Stern-Volmer equation:

$$\tau_0/\tau = 1 + K_q\tau_0 PO_2 \qquad (1)$$

where τ and τ_0 are the measured and zero-oxygen phosphorescence lifetimes, PO_2 is the oxygen tension, and K_q is the second-order rate constant for quenching of phosphorescence.

Figure 2B shows the time course of the activity-dependent oxygen tension changes thus obtained (*23*). The small standard deviations indicate that the changes in oxygen tension in response to a sensory stimulus are reliably detected by this method. The oxygen concentration within the microvasculature

Department of Neurobiology, Center for Research of Higher Brain Functions, Weizmann Institute of Science, Rehovot 76100, Israel.

starts to decline almost as soon as cortical electrical activity is evoked by the stimulus. It reaches its minimum after ~1.5 s and then starts to increase quickly, crossing the baseline after ~2.5 s. The delayed free oxygen increase peaks after 6 s and then begins to decline again. To prove that the onset of the early deoxygenation precedes any blood volume changes, we measured blood volume changes simultaneously with the phosphorescence decay times. The onset of blood volume changes is delayed by ~0.5 s with respect to the onset of changes in oxygen tension (Fig. 2B, inset). This delay rules out the existence of a fast, vein/venule-specific, blood volume increase similar to that predicted by the balloon model at this early time (*24*) that might otherwise provide an alternative explanation for the observed deoxygenation (*21*). These results suggest once again that the first fast event is increased oxygen consumption by the electrically active neurons, followed by a large hyperoxygenation, most probably due to the delayed blood flow increase. The ratio of negative to positive peak is ~4.5 (Fig. 2B), which indicates a large mismatch between oxygen consumption and supply. Having seen similar results in seven independent experiments performed on four cats (Fig. 3C), we conclude that in the anesthetized cat, the first event after a sensory stimulus is a decrease in oxygen saturation due to an increase in oxygen consumption, caused in turn by an increase in oxidative metabolism in electrically active neurons or adjacent glia.

We wondered how the time course of activity-dependent oxygen concentration changes obtained by this direct measurement relates to the indirect measurements obtained by imaging spectroscopy and blood flow measurements (*7, 8*). Under some assumptions (*25*), these changes in the concentration of free oxygen in the microvascular system can be calculated from the relative changes in the concentrations of oxyhemoglobin and deoxyhemoglobin as follows:

$$\Delta[O_2] \propto \Delta[Oxy] - \Delta[Deoxy][Oxy]_0/[Deoxy]_0 \quad (2)$$

where $[Oxy]_0$ and $[Deoxy]_0$ are the oxy- and deoxyhemoglobin concentrations at rest. We analyzed the imaging spectroscopy data at a wavelength range of 530 to 650 nm. The kinetics of activity-dependent changes in the concentrations of oxyhemoglobin and deoxyhemoglobin thus obtained are shown in Fig. 3A. From these results, we estimated the time course of oxygen concentration changes with the use of Eq. 2. Remarkably, the result (Fig. 3B) is qualitatively similar to the time course obtained with our direct measurements (Fig. 3C): Both methods yielded an initial decrease in oxygen, followed by a large hyperoxygenation. Thus, the existence of the initial dip is supported by these two independent measurements.

The present direct measurements of oxygen tension in the cortical microvasculature indicate that the initial dip reflects a very fast increase in oxidative metabolism in response to sensory stimulation. These results are consistent with the fast decrease in NADH (reduced form of nicotinamide adenine dinucleotide) fluorescence reported in slices and in vivo after electrical stimulation (*26*). Recent PET measurements of the human brain have both supported (*27*) and refuted (*13*) this initial increase in oxidative metabolism, as have many previous fMRI measurements (*11*). The present results, rather than reflecting a species difference between feline and primate or the state of anesthesia (*14*), are very relevant to fMRI or PET imaging of the human brain. Indeed, our conclusions have recently been confirmed by 4.7 T fMRI measurements on monkeys (*10*) and by 4 T, 9.4 T, and 4.7 T fMRI measurements on humans and on anesthetized cats (*9*). It has been argued, on theoretical (*24*) and experimental (*28*) bases, that the amplitude of the initial dip seen with fMRI depends on the second power of the field strength. Furthermore, Logothetis has recently shown that the initial dip detected with high-field fMRI in the parenchyma is not detected in the large vessels, whereas the late BOLD component is detected in both compartments [figure 5 in (*10*)]. Why the initial dip has not been observed by most low-field BOLD fMRI measurements is an important question (*28*). It seems that low-field BOLD measurements are not sufficiently sensitive to changes in deoxyhemoglobin concentration in the cortical capillaries. The spatial resolution of such fMRI measurements is therefore not quite clear. Robust ocular dominance columns have been imaged by fMRI only by relying on either differential imaging or signal amplitude (*29*), yet this is not always practical. There is a better solution: It has been shown that the delayed

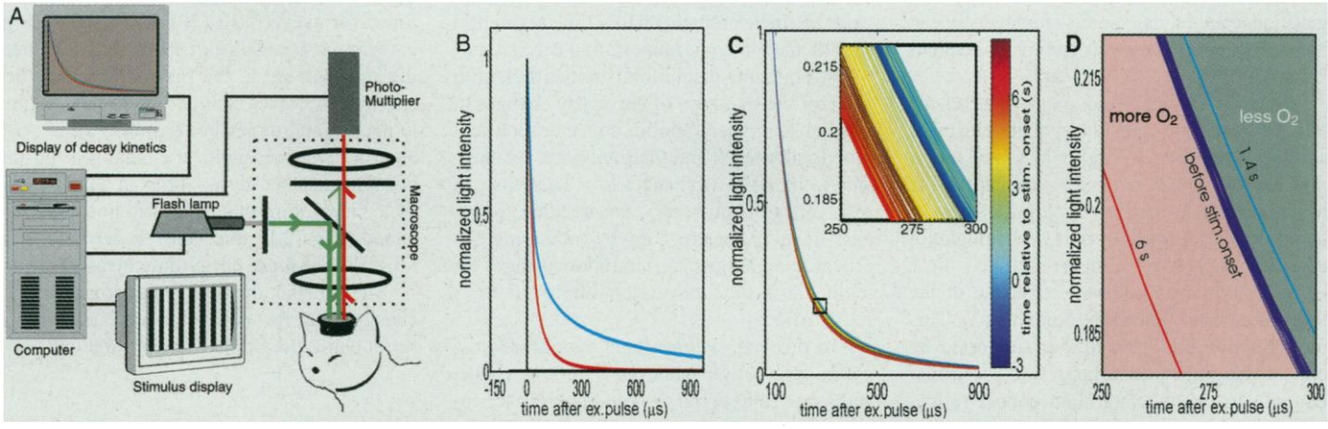

Fig. 1. In vivo oxygen tension measurement by analysis of phosphorescence decay kinetics. **(A)** The setup. Drifting gratings are presented in front of the cat's eyes. Brief pulses are flashed onto the exposed cortex (*18*) through an interference filter (peak transmission 510 nm; bandwidth 10 nm) and are reflected by a dichroic mirror (cutoff at 590 nm) onto a selected region of 2 mm by 2 mm in area 18, devoid of arteries or veins with a diameter of >80 to 100 μm. Flashing rate, 10 Hz. Emitted phosphorescence is collected by a photomultiplier after filtering the light by a 610-nm long-pass filter. The photomultiplier current is used to measure the decay kinetics of the phosphorescence. **(B)** The flash (black line) and two phosphorescence decay curves. The faster one (red) was recorded when the animal was lightly anesthetized; the slower one (blue), showingreduced blood oxygenation, was recorded after injecting additional anesthetics (until the electroencephalogram was nearly flat). **(C)** Decay curves (average of 96 trials) obtained before (dark blue), during (light blue-green), and after (yellow-red) the stimulus. Inset: Detail of the decay curves. **(D)** Expanded display of each of the three phases seen in (C). Dark blue curves: several prestimulus "baseline" decay curves showing the baseline stability. Decay curves above this area (green shading) imply less oxygen, and those below (pink shading) imply more oxygen. The blue curve is a slower decay curve recorded 1.4 s after stimulus onset, showing a decreased oxygen concentration. The red curve was taken 6 s after stimulus onset. It is faster than the baseline decay, showing the delayed hyperoxygenation phase.

blood flow and blood volume changes are not colocalized with activated cortical columns (*7, 8*). Here, we show that the initial dip is a reflection of fast changes in oxidative metabolism. Because changes in oxidative metabolism and in electrical activity are colocalized, it appears that a much better spatial resolution—approaching that obtained with optical imaging—will be achieved using high-field fMRI measurements during the initial dip period. Such a resolution is required to visualize fundamental processing modules performing higher cognitive functions in the human brain.

Note added in proof: The recent visualization of the cat orientation columns by Kim *et al.* (*9*) supports this conclusion.

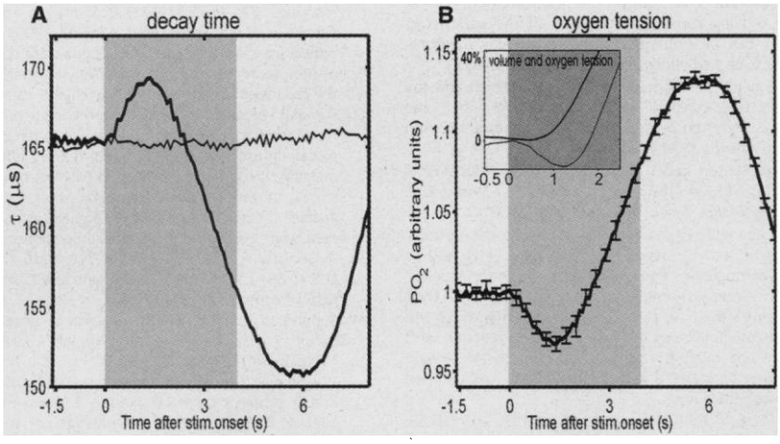

Fig. 2. Activity-dependent phosphorescence decay time and oxygen tension in the cortical microcirculation. Each trial consisted of 95 decay curves, collected every 0.1 s before, during, and after the visual stimulus. The decay constants were obtained by monoexponential fitting (*22*) at the time range of 100 to 500 μs after the flash (*16*). In seven independent experiments on four cats, we obtained $\langle\tau\rangle$ = 181 μs, $\sigma_{\langle\tau\rangle}$ = 15 μs. **(A)** Thick line: decay time constants of the phosphorescence, shown in Fig. 1C, plotted as a function of time with respect to stimulus onset. Thin line: control decay time constants for the decay curves obtained for 9.5 s with same procedure, but without stimulus. Shaded area indicates stimulus time in all panels. **(B)** Oxygen tension as calculated by Eq. 1 from the thick curve in (A). Error bars denote 1 standard deviation of the mean obtained from six independent groups of 16 trials each. Inset: Onset of the activity-dependent blood volume increase is delayed relative to the fast decrease in oxygen concentration. Blood volume changes (thick trace) were measured with optical imaging of the changes in reflected light at an isosbestic wavelength (570 nm), sensitive primarily to blood volume changes. This measurement was performed simultaneously with the phosphorescence measurements (thin trace) from precisely the same cortical area, devoid of any large blood vessels. These two curves were normalized to their peak amplitudes (100%; not shown in the inset) occurring after 6 s in both cases.

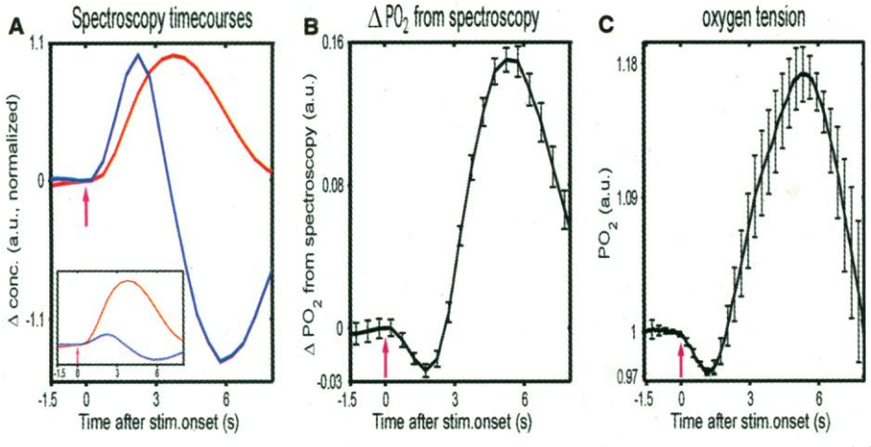

Fig. 3. Calculation of the time course of changes in oxygen tension from imaging spectroscopy. **(A)** Time course of activity-dependent changes in oxyhemoglobin (red) and deoxyhemoglobin (blue) concentration obtained with imaging spectroscopy. Curves were normalized for easier comparison of timing relations. The inset shows the observed curves without normalization. Arrows: stimulus onset in all panels. **(B)** Activity-dependent changes in oxygen tension estimated from imaging spectroscopy. See text and (*25*) (n = 8; error bars: SD of the mean). **(C)** Oxygen tension observed with phosphorescence; means and SD are from seven independent experiments on four cats. The timing of the deoxygenation phase peak measured by the two methods was similar but not identical, presumably because of the approximations used in the analysis of imaging spectroscopy (*14, 25*), its low time resolution, and the variability observed in different experiments.

References and Notes

1. P. T. Fox *et al.*, *Nature* **323**, 806 (1986); P. T. Fox, F. M. Miezin, J. M. Allman, D. C. Van Essen, M. E. Raichle, *J. Neurosci.* **7**, 913 (1987); J. W. Belliveau *et al.*, *Science* **254**, 716 (1991); M. I. Sereno *et al.*, *Science* **268**, 889 (1995); E. A. DeYoe *et al.*, *Proc. Natl. Acad. Sci. U.S.A.* **93**, 2382 (1996); R. H. B. Tootell *et al.*, *J. Neurosci.* **15**, 3215 (1997); S. A. Engel, G. H. Glover, B. A. Wandell, *Cereb. Cortex* **7**, 181 (1997).
2. S. Ogawa *et al.*, *Proc. Natl. Acad. Sci. U.S.A.* **89**, 5951 (1992); K. K. Kwong *et al.*, *Proc. Natl. Acad. Sci. U.S.A.* **89**, 5675 (1992); R. Turner *et al.*, *Magn. Reson. Med.* **29**, 277 (1993).
3. D. Y. Ts'o, R. D. Frostig, E. D. Lieke, A. Grinvald, *Science* **240**, 333 (1990). T. Bonhoeffer and A. Grinvald, *Nature* **353**, 429 (1991); G. Wang, K. Tanaka, M. Tanifuji, *Science* **272**, 1665 (1996).
4. E. Bartfeld and A. Grinvald, *Proc. Natl. Acad. Sci. U.S.A.* **89**, 11905 (1992); A. Shmuel and A. Grinvald, *J. Neurosci.* **16**, 6945 (1996); M. Weliky, W. H. Bosking, D. Fitzpatrick, *Nature* **379**, 725 (1996); M. Hubener, D. Shoham, A. Grinvald, T. Bonhoeffer, *J. Neurosci.* **17**, 9270 (1997).
5. C. Roy and C. Sherrington, *J. Physiol.* **11**, 85 (1890); S. S. Kety, W. M. Landau, L. P. Rowland, L. Sokoloff, *Am. Soc. Physiol. Abstr.* **85** (1955); A. Lassen and D. H. Ingvar, *Experimentia Basel* **17**, 42 (1961); M. Kato, H. Ueno, P. Black, *J. Cereb. Blood Flow Metab.* **42**, 65 (1974); L. Sokoloff, *J. Neurochem.* **29**, 13 (1977); I. Silver, *Ciba Found. Symp.* **56**, 49 (1978); P. Fox and M. Raichle, *Ann. Neurol.* **17**, 303 (1985); H. Lou, L. Edvinsson, E. MacKenzie, *Ann. Neurol.* **22**, 289 (1987); C. Iadecola, *Trends Neurosci.* **16**, 206 (1993).
6. P. T. Fox, M. E. Raichle, M. A. Mintun, C. Dence, *Science* **241**, 462 (1988).
7. A. Grinvald, E. Lieke, R. D. Frostig, C. D. Gilbert, T. N. Wiesel, *Nature* **324**, 361 (1986); R. D. Frostig, E. Lieke, D. Y. Ts'o, A. Grinvald, *Proc. Natl. Acad. Sci. U.S.A.* **87**, 6082 (1990); D. Malonek *et al.*, *Proc. Natl. Acad. Sci. U.S.A.* **94**, 14826 (1997).
8. D. Malonek and A. Grinvald, *Science* **272**, 551 (1996).
9. X. Hu, T. H. Le, K. Ugurbil, *Magn. Reson. Med.* **37**, 877 (1997); E. Yacoub, T. H. Le, K. Ugurbil, X. Hu, *Magn. Reson. Med.* **41**, 436 (1999); D.-S. Kim, T. Q. Duong, S.-G. Kim, *Neurosci. Abstr.* **25**, 783 (1999).
10. N. Logothetis *et al.*, *Nature Neurosci.* **2**, 555 (1999).
11. P. Fransson, G. Kruger, K. D. Merboldt, J. Frahm, *Magn. Reson. Med.* **39**, 912 (1998); J. Frahm, G. Krueger, K. D. Merboldt, A. Kleinschmidt, *Adv. Exp. Med. Biol.* **413**, 195 (1997); G. Kruger, A. Kleinschmidt, J. Frahm, *Magn. Reson. Med.* **35**, 797 (1996); J. J. A. Marota *et al.*, *Magn. Reson. Med.* **41**, 247 (1999); A. Kleinschmidt *et al.*, *J. Cereb. Blood Flow Metab.* **16**, 817 (1996); F. Hyder *et al.*, *Proc. Natl. Acad. Sci. U.S.A.* **93**, 7612 (1996).
12. J. E. W. Mayhew, *Neuroimage* **7**, 49 (1998); M. Nemoto, *J. Cereb. Blood Flow Metab.* **19**, 246 (1999); J. Mayhew *et al.*, *Neuroimage* **10**, 304 (1999).
13. H. Fujita, H. Kuwabara, D. C. Reutens, A. Gjedde, *J. Cereb. Blood Flow Metab.* **19**, 266 (1999).
14. The spectrum of the light reflected from the cortex depends on (i) the spectra of the intrinsic chromophores, (ii) their concentration, and (iii) the distance the light travels in the medium. In a scattering medium like cortical tissue, this path length depends on both the scattering and the absorption properties. It is therefore wavelength-dependent. Malonek and Grinvald have used a simplified linear equation in which the path length was assumed constant, and with their simplified model, the initial dip was observed in the anesthetized cat (*8*) and the awake behaving primate (E. Shtoyerman, I. Vanzetta, A. Grinvald, unpublished data). An alternative, more rigorous approach has been proposed recently by Mayhew and colleagues; the initial dip was also observed in the rat whisker barrel system using their

model, after subtraction of the vasomotion signals (*12*). We also analyzed several data sets from different species at the full wavelength range using a more rigorous algorithm similar to that proposed by Mayhew. We found that the initial dip persisted or disappeared depending on the parameters used in the model, and the residuals of the curve fitting could not be used as reliable criteria for the validity of the model parameters [U. Lindauer *et al.*, *Neurosci. Abstr.* **25**, 1639 (1999)].

15. D. F. Wilson, W. L. Rumsey, T. J. Green, J. M. Vanderkooi, *J. Biol. Chem.* **263**, 2712 (1983); W. L. Rumsey, J. M. Vanderkooi, D. F. Wilson, *Science* **241**, 1649 (1988); D. F. Wilson *et al.*, *Adv. Exp. Med. Biol.* **215**, 71 (1987); D. F. Wilson, *Adv. Exp. Med. Biol.* **333**, 225 (1993); S. A. Vinogradov and D. F. Wilson, *Adv. Exp. Med. Biol.* **361**, 67 (1994).
16. I. P. Torres Filho and M. Intaglietta, *Am. J. Physiol.* **265**, H1434 (1993); H. Kerger, I. P. Torres Filho, M. Rivas, R. M. Winslow, M. Intaglietta, *Am. J. Physiol.* **268**, H802 (1995); M. Pawlowski and D. F. Wilson, *Adv. Exp. Med. Biol.* **316**, 179 (1999).
17. L.-W. Lo, C. J. Koch, D. F. Wilson, *Anal. Biochem.* **236**, 153 (1996); L.-W. Lo, S. A. Vinogradov, C. J. Koch, D. F. Wilson, *Adv. Exp. Med. Biol.* **428**, 651 (1997).
18. All surgical and experimental procedures were in accordance with NIH guidelines. Details are described elsewhere (*7, 8*). Cats were anesthetized during the recording phase with continuous infusion of sodium pentothal. A craniotomy overlying area 18 of the visual cortex was performed and the dura removed. Stimulation protocol: (i) blank screen (prestimulus time, 1.5 to 5 s); (ii) moving gratings for 4 s (high contrast, 0.2 cycles per degree, duty cycle = 0.3, 6 cycles per second), and (iii) a blank screen (poststimulus time, at least 30 s). Up to 96 such trials were averaged.
19. E. H. Ratzlaff and A. Grinvald, *J. Neurosci. Methods* **36**, 127 (1991). Instead of a tungsten halogen lamp, we used a flash lamp (flash lamp model LABPAC 1200 power supply, with trigger unit LITE-PAC FYD-1150 and flashtube FX-1150, providing a flash of 3 μs exponential decay time; EG&G Electro Optics, Salem, MA).
20. H. Kerger *et al.*, *Anesthesiology* **86**, 372 (1997).
21. The other factors affecting the phosphorescence decay time are temperature, salinity, and pH. By their nature, salinity and temperature changes are much slower than the phenomenon under examination. The upper limit for a pH change should be smaller than the arterovenous pH difference of $\Delta pH = 0.03$. Using pH calibration data (*17*), the effect of ΔpH (pH = 7.4 was taken as the resting pH) on the decay time is negligible, about 7% of the difference we observed during the deoxygenation phase. The initial dip detected with phosphorescence decay time measurements cannot be attributed to blood volume rearrangements among microvascular compartments, because the latter's onset is delayed by ~500 ms (Fig. 2B, inset). In addition, in those high-resolution volume measurements (4 μm), the volume increase observed in venules and veins was neither faster nor larger than in the other compartments. Previous (*7, 19*) and recent (I. Vanzetta, R. Hildesheim, A. Grinvald, unpublished data) fluorescent tracer imaging measurements confirmed these results. The visualization of a stimulus-dependent increase in red blood cell velocity in individual capillaries [D. Kleinfeld, P. P. Mitra, F. Helmchen, W. Denk, *Proc. Natl. Acad. Sci. U.S.A.* **95**, 15741 (1998)], also showed that the flow increase starts late (> ~0.5 s).
22. A weighted nonlinear least squares analysis was used to obtain the decay parameters (*30*). At least three exponential components are expected for the three vascular compartments. However, the true decay function is even more complex; in each compartment a wide distribution was found (*16*). However, a single exponential-fit approximation is sufficient to show the initial decrease in oxygen tension claimed here. The graphs in Fig. 2 are based on such fit. To rule out the possibility that the observed increase in activity-dependent decay time is not an artifact of the single component fit to a complex decay function, we also performed multicomponent analyses. For a two-components fit we obtained $\tau_1 = 65.9 \pm 0.3$ μs, $\tau_2 = 274 \pm 1$ μs, with amplitudes of $A_1 = 67.1 \pm 0.5\%$ and $A_2 = 32.9 \pm 0.5\%$. The initial dip was clearly present and statistically significant (95% confidence) in the time course of the shortest decay time. For three-components analysis, the initial dip was observed in the second component. However, as expected, the same goodness of fit was provided by very different decay parameters. For example set 1: $\tau_1 = 24$ μs, $\tau_2 = 70$ μs, $\tau_3 = 281$ μs, $A_1 = 5\%$, $A_2 = 63\%$, $A_3 = 32\%$; set 2: $\tau_1 = 59$ μs, $\tau_2 = 182$ μs, $\tau_3 = 620$ μs, $A_1 = 57\%$, $A_2 = 36\%$, $A_3 = 7\%$. These large differences underscore the inherent ambiguities of multiexponential analysis [(*30*) and references therein]. Adding constraints to some of the parameters that can be obtained from independent measurements should allow more quantitative analysis.
23. The decay constant at zero oxygen tension and the quenching constant were taken for pH = 7.4 and 38°C body temperature, 4% albumin, and 120 mM NaCl from published values (*17*).
24. R. B. Buxton and L. R. Frank, *J. Cereb. Blood Flow Metab.* **17**, 64 (1997); R. B. Buxton, E. C. Wong, L. R. Frank, *Magn. Reson. Med.* **39**, 855 (1998).
25. Obtaining Eq. 2 required the following assumptions: (i) The activity-dependent changes in P_{O_2} and in oxyhemoglobin and deoxyhemoglobin concentrations were assumed to be small relative to their resting values; (ii) the cooperative binding of oxygen to hemoglobin was approximated by a reaction with constant binding strength; and (iii) mean oxygen saturation in the sampled blood volume was assumed to be ~85%.
26. B. Chance and B. Schoener, *Nature* **195**, 956 (1962); P. Lipton, *Biochem. J.* **136**, 999 (1973); E. Lothmann, J. LaManna, G. Cordingley, M. Rosenthal, G. Somjen, *Brain Res.* **88**, 15 (1975).
27. G. Blomqvist *et al.*, *Acta Physiol. Scand.* **151**, 29 (1994); M. S. Vafaee *et al.*, *J. Cereb. Blood Flow Metab.* **19**, 272 (1999).
28. It has been argued on theoretical (*24*) as well as experimental grounds (comparing the amplitude of the dip at 1.5 and 4 T) that the amplitude of the initial dip seen with fMRI depends on the second power of the field strength (K. Ugurbil, personal communication).
29. R. S. Menon, S. Ogawa, J. P. Strupp, K. Ugurbil, *J. Neurophysiol.* **77**, 2780 (1997); R. S. Menon and B. G. Goodyear, *Magn. Reson. Med.* **41**, 230 (1999). As with optical imaging, the fMRI BOLD signals are composed of (i) a "local" component, most likely originating from the capillaries situated in the parenchyma, carrying the stimulus' specificity; and (ii) a component originating from other sources, such as large veins, having more global diffuse character. For this reason, differential imaging comparing the activation patterns of different stimuli known to activate "orthogonal" cortical regions enables the enhancement of the signals' local component while getting rid of the global component.
30. A. Grinvald, E. Haas, I. Steinberg, *Proc. Natl. Acad. Sci. U.S.A.* **69**, 2273 (1972); A. Grinvald and I. Steinberg, *Anal. Biochem.* **59**, 583 (1974).
31. Supported by a grant from the German Israeli Foundation. We thank R. Buxton, U. Dirnagl, N. Logothetis, I. Steinberg, R. B. H. Tootell, K. Ugurbil, and D. F. Wilson for their useful suggestions and comments, and D. Ettner, I. Lampl, D. Nelson, E. Shtoyerman, D. Sharon, H. Slovin, and C. Wijnbergen for their help during the experiments.

30 June 1999; accepted 14 October 1999

Transmission of Chronic Nociception by Spinal Neurons Expressing the Substance P Receptor

Michael L. Nichols,[1,2] Brian J. Allen,[1,2] Scott D. Rogers,[1,2] Joseph R. Ghilardi,[1,2] Prisca Honore,[1,2] Nancy M. Luger,[1,2] Matthew P. Finke,[1,2] Jun Li,[1] Douglas A. Lappi,[3] Donald A. Simone,[1] Patrick W. Mantyh[1,2]*

Substance P receptor (SPR)–expressing spinal neurons were ablated with the selective cytotoxin substance P–saporin. Loss of these neurons resulted in a reduction of thermal hyperalgesia and mechanical allodynia associated with persistent neuropathic and inflammatory pain states. This loss appeared to be permanent. Responses to mildly painful stimuli and morphine analgesia were unaffected by this treatment. These results identify a target for treating persistent pain and suggest that the small population of SPR-expressing neurons in the dorsal horn of the spinal cord plays a pivotal role in the generation and maintenance of chronic neuropathic and inflammatory pain.

Chronic pain conditions are caused by ongoing disease states or tissue damage that result in sensitization of primary afferent and spinal cord neurons. This sensitization results in an increased sensitivity to both noxious (hyperalgesia) and non-noxious (allodynia) stimuli that is frequently difficult to treat with current pharmacological or surgical approaches (*1*).

Spinothalamic (STT) and spinoparabrachial (SPB) neurons are involved in the ascending conduction of acute noxious stimuli. Sensitization of these neurons results in hyperalgesia (*2*). Although SPR-expressing neurons represent less than 5% of the total neurons in the dorsal horn of the spinal cord

[1]Departments of Preventive Sciences, Psychiatry, and Neuroscience and Cancer Center, University of Minnesota, Minneapolis, MN 55455, USA. [2]Molecular Neurobiology Lab (151), Veterans Affairs Medical Center, Minneapolis, MN 55417, USA. [3]Advanced Targeting Systems, 11175-A Flintkote Avenue, San Diego, CA 92121, USA.

*To whom correspondence should be addressed. E-mail: manty001@maroon.tc.umn.edu

References and Notes

[1] **Functional Mapping of the Human Visual Cortex by Magnetic Resonance Imaging**

J. W. Belliveau; D. N. Kennedy; R. C. McKinstry; B. R. Buchbinder; R. M. Weisskoff; M. S. Cohen; J. M. Vevea; T. J. Brady; B. R. Rosen

Science, New Series, Vol. 254, No. 5032. (Nov. 1, 1991), pp. 716-719.

Stable URL:

http://links.jstor.org/sici?sici=0036-8075%2819911101%293%3A254%3A5032%3C716%3AFMOTHV%3E2.0.CO%3B2-F

[1] **Borders of Multiple Visual Areas in Humans Revealed by Functional Magnetic Resonance Imaging**

M. I. Sereno; A. M. Dale; J. B. Reppas; K. K. Kwong; J. W. Belliveau; T. J. Brady; B. R. Rosen; R. B. H. Tootell

Science, New Series, Vol. 268, No. 5212. (May 12, 1995), pp. 889-893.

Stable URL:

http://links.jstor.org/sici?sici=0036-8075%2819950512%293%3A268%3A5212%3C889%3ABOMVAI%3E2.0.CO%3B2-V

[1] **Mapping Striate and Extrastriate Visual Areas in Human Cerebral Cortex**

Edgar A. DeYoe; George J. Carman; Peter Bandettini; Seth Glickman; Jon Wieser; Robert Cox; David Miller; Jay Neitz

Proceedings of the National Academy of Sciences of the United States of America, Vol. 93, No. 6. (Mar. 19, 1996), pp. 2382-2386.

Stable URL:

http://links.jstor.org/sici?sici=0027-8424%2819960319%2993%3A6%3C2382%3AMSAEVA%3E2.0.CO%3B2-0

LINKED CITATIONS

[2] **Intrinsic Signal Changes Accompanying Sensory Stimulation: Functional Brain Mapping with Magnetic Resonance Imaging**

Seiji Ogawa; David W. Tank; Ravi Menon; Jutta M. Ellermann; Seong-Gi Kim; Hellmut Merkle; Kamil Ugurbil

Proceedings of the National Academy of Sciences of the United States of America, Vol. 89, No. 13. (Jul. 1, 1992), pp. 5951-5955.

Stable URL:

http://links.jstor.org/sici?sici=0027-8424%2819920701%2989%3A13%3C5951%3AISCASS%3E2.0.CO%3B2-4

[2] **Dynamic Magnetic Resonance Imaging of Human Brain Activity During Primary Sensory Stimulation**

Kenneth K. Kwong; John W. Belliveau; David A. Chesler; Inna E. Goldberg; Robert M. Weisskoff; Brigitte P. Poncelet; David N. Kennedy; Bernice E. Hoppel; Mark S. Cohen; Robert Turner; Hong-Ming Cheng; Thomas J. Brady; Bruce R. Rosen

Proceedings of the National Academy of Sciences of the United States of America, Vol. 89, No. 12. (Jun. 15, 1992), pp. 5675-5679.

Stable URL:

http://links.jstor.org/sici?sici=0027-8424%2819920615%2989%3A12%3C5675%3ADMRIOH%3E2.0.CO%3B2-B

[3] **Functional Organization of Primate Visual Cortex Revealed by High Resolution Optical Imaging**

Daniel Y. Ts'o; Ron D. Frostig; Edmund E. Lieke; Amiram Grinvald

Science, New Series, Vol. 249, No. 4967. (Jul. 27, 1990), pp. 417-420.

Stable URL:

http://links.jstor.org/sici?sici=0036-8075%2819900727%293%3A249%3A4967%3C417%3AFOOPVC%3E2.0.CO%3B2-Z

[3] **Optical Imaging of Functional Organization in the Monkey Inferotemporal Cortex**

Gang Wang; Keiji Tanaka; Manabu Tanifuji

Science, New Series, Vol. 272, No. 5268. (Jun. 14, 1996), pp. 1665-1668.

Stable URL:

http://links.jstor.org/sici?sici=0036-8075%2819960614%293%3A272%3A5268%3C1665%3AOIOFOI%3E2.0.CO%3B2-A

LINKED CITATIONS

[4] **Relationships Between Orientation-Preference Pinwheels, Cytochrome Oxidase Blobs, and Ocular-Dominance Columns in Primate Striate Cortex**

Eyal Bartfeld; Amiram Grinvald

Proceedings of the National Academy of Sciences of the United States of America, Vol. 89, No. 24. (Dec. 15, 1992), pp. 11905-11909.

Stable URL:

http://links.jstor.org/sici?sici=0027-8424%2819921215%2989%3A24%3C11905%3ARBOPCO%3E2.0.CO%3B2-T

[6] **Nonoxidative Glucose Consumption during Focal Physiologic Neural Activity**

Peter T. Fox; Marcus E. Raichle; Mark A. Mintun; Carmen Dence

Science, New Series, Vol. 241, No. 4864. (Jul. 22, 1988), pp. 462-464.

Stable URL:

http://links.jstor.org/sici?sici=0036-8075%2819880722%293%3A241%3A4864%3C462%3ANGCDFP%3E2.0.CO%3B2-C

[7] **Cortical Functional Architecture and Local Coupling Between Neuronal Activity and the Microcirculation Revealed by In vivo High-Resolution Optical Imaging of Intrinsic Signals**

Ron D. Frostig; Edmund E. Lieke; Daniel Y. Ts'o; Amiram Grinvald

Proceedings of the National Academy of Sciences of the United States of America, Vol. 87, No. 16. (Aug., 1990), pp. 6082-6086.

Stable URL:

http://links.jstor.org/sici?sici=0027-8424%28199008%2987%3A16%3C6082%3ACFAALC%3E2.0.CO%3B2-R

[7] **Vascular Imprints of Neuronal Activity: Relationships between the Dynamics of Cortical Blood Flow, Oxygenation, and Volume Changes Following Sensory Stimulation**

Dov Malonek; Ulrich Dirnagl; Ute Lindauer; Katsuya Yamada; Iwao Kanno; Amiram Grinvald

Proceedings of the National Academy of Sciences of the United States of America, Vol. 94, No. 26. (Dec. 23, 1997), pp. 14826-14831.

Stable URL:

http://links.jstor.org/sici?sici=0027-8424%2819971223%2994%3A26%3C14826%3AVIONAR%3E2.0.CO%3B2-V

[8] **Interactions between Electrical Activity and Cortical Microcirculation Revealed by Imaging Spectroscopy: Implications for Functional Brian Mapping**

Dov Malonek; Amiram Grinvald

Science, New Series, Vol. 272, No. 5261. (Apr. 26, 1996), pp. 551-554.

Stable URL:

http://links.jstor.org/sici?sici=0036-8075%2819960426%293%3A272%3A5261%3C551%3AIBEAAC%3E2.0.CO%3B2-E

LINKED CITATIONS

[11] **Increased Tricarboxylic Acid Cycle Flux in Rat Brain during Forepaw Stimulation Detected with ¹ H [¹³ C] NMR**

Fahmeed Hyder; Jennifer R. Chase; Kevin L. Behar; Graeme F. Mason; Mohamed Siddeek; Douglas L. Rothman; Robert G. Shulman

Proceedings of the National Academy of Sciences of the United States of America, Vol. 93, No. 15. (Jul. 23, 1996), pp. 7612-7617.

Stable URL:

http://links.jstor.org/sici?sici=0027-8424%2819960723%2993%3A15%3C7612%3AITACFI%3E2.0.CO%3B2-P

[15] **Imaging of Phosphorescence: A Novel Method for Measuring Oxygen Distribution in Perfused Tissue**

William L. Rumsey; Jane M. Vanderkooi; David F. Wilson

Science, New Series, Vol. 241, No. 4873. (Sep. 23, 1988), pp. 1649-1651.

Stable URL:

http://links.jstor.org/sici?sici=0036-8075%2819880923%293%3A241%3A4873%3C1649%3AIOPANM%3E2.0.CO%3B2-6

[21] **Fluctuations and Stimulus-Induced Changes in Blood Flow Observed in Individual Capillaries in Layers 2 through 4 of Rat Neocortex**

David Kleinfeld; Partha P. Mitra; Fritjof Helmchen; Winfried Denk

Proceedings of the National Academy of Sciences of the United States of America, Vol. 95, No. 26. (Dec. 22, 1998), pp. 15741-15746.

Stable URL:

http://links.jstor.org/sici?sici=0027-8424%2819981222%2995%3A26%3C15741%3AFASCIB%3E2.0.CO%3B2-N

[30] **Evaluation of the Distribution of Distances between Energy Donors and Acceptors by Fluorescence Decay**

A. Grinvald; E. Haas; I. Z. Steinberg

Proceedings of the National Academy of Sciences of the United States of America, Vol. 69, No. 8. (Aug., 1972), pp. 2273-2277.

Stable URL:

http://links.jstor.org/sici?sici=0027-8424%28197208%2969%3A8%3C2273%3AEOTDOD%3E2.0.CO%3B2-1